A Gibbs Energy Balance Model for Growth Via Diffusional Growth-Ledges

Clark, S., Lan, Y., Rahnama, A., Janik, V. & Sridhar, S.

DOI 10.2355/isijinternational.ISIJINT-2018-621
ISSN 0915-1559

Publisher: Iron & Steel Institute of Japan

A Gibbs Energy Balance Model for Growth Via Diffusional Growth-Ledges

Authors

SAMUEL JAMES CLARK, YONGJUN LAN, ALIREZA RAHNAMA, VIT JANIK, SEETHARAMAN SRIDHAR

Corresponding Author: SAMUEL JAMES CLARK – Email: samuel.clark@ucl.ac.uk

Author Affiliations

SAMUEL JAMES CLARK: Mechanical Engineering, University College London, Torrington Place, London, WC1E 7JE, UK.

YONGJUN LAN: Tata Steel, Coventry Technology Centre, Coventry CV4 7EZ, United Kingdom.

ALIREZA RAHNAMA, AI Manufacturing Solutions, 1 Sandover House, 124 Spa Road, London, SE16 3FD, UK.

VIT JANIK: Centre for Manufacturing and Materials Engineering, Coventry University, Priory Street, Coventry CV1 5FB, UK.

SEETHARAMAN SRIDHAR, Department of Metallurgical & Materials Engineering, Colorado School of Mines, 1500 Illinois Street Golden, Colorado 8040, USA.

Key Words

Growth Ledges, Solute Drag, Interphase Precipitation.

Abstract

Growth ledges are commonly observed on interphase boundaries during diffusional phase transformations and are of great importance for understanding inter-sheet spacing of interphase precipitates. A simple model based on Gibbs Energy Balance (GEB) for describing growth kinetics via diffusional growth-ledges of height λ is presented for the case of ferrite growth into austenite. The model is validated against the case of austenite to ferrite transformation involving interphase precipitation in a V, Mn, Si alloyed HSLA steel where, λ is assumed to be equal to the inter-sheet spacing of interphase carbide precipitates. The presented model provides a computationally efficient and versatile method for predicting the ledge height, λ, and the growth kinetics of ferrite from initial nucleation through to final soft impingement considering the evolution of solute drag at growth ledge risers. It is suggested that the intrinsic mobility of growth ledge risers is: $M_m^{\alpha R} = 0.58exp\left(\frac{-140\times10^3}{RT}\right)\ mmol.J^{-1}\ s^{-1}$, with R the gas constant and T the absolute temperature in K.

1. Introduction

Ever since Aaronson forwarded the "theory of precipitate morphology", which proposed that semi-coherent precipitates grow via a ledge mechanism [1], Ledges and ledge-like features have been widely observed during the austenite to ferrite ($\gamma \rightarrow \alpha$) phase transformation in steels [2–4] using different experimental methods, including *in-situ* using hot-stage TEM [5]. However, relatively little is definitively known about their formation and progression and relationship to observed motilities of γ/α interphase boundaries [6–10]. This is in part attributable to the significant experimental difficulty in observing *in-situ* transformations with sufficient resolution both spatially and temporally [10].

A growth ledge, when simplified to a 2D problem, consists of a semi-coherent γ/α interphase boundary, made up of a disordered mobile riser and a comparatively coherent and immobile tread [6]. Smith [11] suggested, an α allotriomorph growing into two neighboring parent γ grains should only exhibit a semi-coherent orientation relationship (OR) with one parent γ grain. This would suggest that a ledge mechanism should only be observed on this semi-coherent side of the growing allotriomorph whereas, on the side growing into the other parent γ grain exhibiting no OR should exhibit a smooth curved incoherent γ/α interphase boundary. During the $\gamma \rightarrow \alpha$ phase transformation two semi-coherent orientation relationships frequently detected are the Kurdjumov-Sachs (KS) [12], or the Nishiyama-Wasserman (NW) [13,14] OR. Edmonds and Honeycombe [3] however, observed using photoemission electron microscopy, faceted and possibly ledged interphase boundaries irrelevant of γ/α OR, with considerable variation in step heights during the growth of allotriomorphic α. This lead Honeycombe [15] to conclude that the 'migration of truly curved high energy ferrite/austenite boundaries is rare and likely only to occur at higher transformation temperatures'.

Interphase precipitation, which is characterized by periodic parallel planes of randomly distributed carbide precipitates ϵ, which form at the moving interphase boundary between γ and α [16] in alloys where a strong carbide forming element is present such as V, Nb or Ti [17]. Davenport and Honeycombe [16], observed interphase precipitation to be associated with $\gamma \rightarrow \alpha$ decomposition via a ledge mechanism. The stationary low energy treads of the ledged α terrace were observed to be marked by the presence of interphase carbide precipitates, which are considered to be offer a greater likelihood of successful ϵ precipitate nucleation than either ledge risers or planar disordered interphase boundaries [18]. Since this observation, ledge terraces during interphase precipitation have been recorded on many occasions [19–21]. Yen *et al.* [21], where fig. 3 (B) clearly shows a ledged terrace on what would be conventionally seen as an incoherent γ/α interphase boundary. The likelihood of this finding was previously discussed by Furuhara and Aaronson [22] in light of experimental results in the Ti-Cr system (precipitation of a HCP phase in a BCC matrix) [23,24], which suggested the presence of growth ledges on the side of the allotriomorph regardless orientation relationship with the parent matrix grain. This result was confirmed by Furuhara and Maki for precipitation of BCC in an FCC matrix for a Ni-Cr alloy [25].

The generality of transformations via a ledge mechanism has been proposed, in particular by Cahn [26] who stated that 'the mechanism of the motion of an interface in a crystalline material depends on the driving force rather than on the crystallographic nature of the interface. At sufficiently large driving forces, the interface can move uniformly'. However, at 'sharp interfaces the necessary driving force is so large that it may be difficult to achieve'. More recently the incoherency view has received renewed attention, Massalski *et al.* [27] reviewed the experimental and theoretical nature of interphase boundaries concluding that an incoherent

boundary may be facetted on various length scales. For the purposes of this study, it will be assumed that all the γ/α interphase boundaries regardless of crystallographic OR exhibit growth ledges.

Diffusional growth ledges in Fe-C alloys are thought to form either: at junctions between grain boundary allotriomorphs and secondary sideplates (boundaries) or via a mechanism where the volume change distorts the path of boundary, creating a ledge [28]. The direct nucleation of growth ledges at boundaries, 2D nucleation, is considered to be the simplest mechanism for ledge formation [29]. A 2D model for the heterogeneous nucleation of diffusional super-ledges was suggested by Bhadeshia [30]. Bhadeshia proposed Equation 1, which states that the critical height for the successful nucleation of a α super-ledge upon an γ/α interphase boundary (which is assumed to be equal to the inter-sheet spacing, λ, in the case of interphase precipitation), is controlled by the interfacial energy of the facet plane of the ledged interphase boundary, σ, the driving force for the transformation, $\Delta G_m^{\gamma\to\alpha}$

$$\lambda = \frac{\sigma V_m}{\Delta G_m^{\gamma\to\alpha}} \quad (1)$$

were, V_m is the molar volume (in this work V_m is taken to be the molar volume for α determined using the Matcalc property database [31]). Although as proposed, this approach was able to predict the trend of refining inter-sheet spacing with reducing temperature excellently, there was still separation between the expected and predicted curves. We previously proposed an adaption of this model, where $\Delta G_m^{\gamma\to\alpha}$ was re-evaluated and enabled to vary throughout the transformation according to a Gibbs Energy Balance (GEB) algorithm. This allowed for the prediction of the evolution of inter-sheet-spacing of interphase carbides in multi-component

alloys [32]. It was shown that the general trend of refining inter-sheet spacing with growing α half-thickness can be well predicted by the proposed model.

However, the α fraction transformed at $973\ K$ in the V-HSLA considered was simulated to increase from 0 to $90\ \%$ within $25\ s$, which was only in general agreement with the kinetics measured using dilatometry. Additionally, the calculated final α fraction was greater than the measured from optical microscopy. It was concluded that the previous model could only predict the velocity of γ/α correctly in terms of an order of magnitude. Furthermore, the model did not address the location of the formation of the growth ledges, rather only provided an estimation of the magnitude of the growth ledges upon an effectively planar interphase.

The principle purpose of the current work is to address the shortcomings in the previous work, it is hypothesized that expanding the model to a more geometrically representative model of the $\gamma \rightarrow \alpha$ phase transformation and evaluating the Gibbs energy balance at growth ledge growth with yield a significantly improved prediction of $\gamma \rightarrow \alpha$ transformation kinetics.

1. The Quasi-1D Model

1.1. Geometric Description of Ledged Interphase Interfaces

Figure 1

Figure 1 shows a schematic depiction of an α ledge terrace which has nucleated at an γ grain boundary corner. In this figure, the horizontal dimension of a ledge named *treads*, and form a

near coherent interface with the parent γ. The vertical dimension of ledge is named the *riser* and have a disordered incoherent interface with γ. Ledges of riser height, λ, are envisaged to heterogeneously nucleate at boundaries, initially at the γ grain boundary corner, then the junction between the γ grain boundary and the tread of the α ledge and finally the junction between α ledge treads when all the γ grain boundary has been consumed. Each of these sites is assumed to have no influence upon the ledge height predicted by Equation 1. at grain boundaries to the left. The ledges move at a velocity v_L towards the right, the ledges are assumed not to change in height as they move as the more coherent, low energy ledged γ/α boundary tread is considered to be immobile [6], i.e. $v_T \approx 0$. The ledges are considered to repulse one another through a strong repulsive elastic interaction attributable to the change in molar volume from the transformation. This elastic interaction term decreases with inter-ledge spacing (ledge tread distance), τ [33]. It is additionally considered that this elastic repulsion is proportional to the height of the ledge riser, λ. Under such conditions, characteristic ledge riser to tread ratio $\left(\frac{\lambda}{\tau}\right)$ develops, and all the ledge risers must be travelling at the same velocity for this to be maintained.

The heterogeneous nucleation rate of ledges is assumed not to be rate limiting. Rather a ledge which has nucleated at a boundary (dashed ledge at the left) only becomes mobile once the previous ledge riser has traversed a sufficient distance to the right, such that the elastic repulsion caused by the previous ledge has sufficiently diminished. Under such assumptions, there is a constant relationship between ledge height and ledge tread.

Several models have been proposed for growth ledges for either individual ledges or trains or multiple ledges, notably the work of Atkinson [34,35] and Enomoto and co workers [36–39]. Of particular relevance to this study is the finding in Fig 2. [38] that ledge growth is well

approximated by a planar disordered interphase when the ledge height to tread length ratio $\left(\frac{\lambda}{\tau}\right)$ is large as the carbon diffusion field around the ledge risers overlap. Enomoto compared two cases where $\left(\frac{\lambda}{\tau}\right) = \frac{1}{2}$ and $\frac{1}{50}$. In both cases the growth kinetics were found to eventually converge with that of the planar disordered interphase model however, in the case of $\left(\frac{\lambda}{\tau}\right) = \frac{1}{50}$ this was found to occur only after a long period of time. Okamoto and Agren [40] extracted values for $\left(\frac{\lambda}{\tau}\right)$ of between $\frac{1}{3.6}$ and $\frac{1}{4.6}$ (i.e. $\phi = 0.271 - 0.214\, rad.$) from TEM micrographs of partial decompositions of $\gamma \rightarrow \alpha + \epsilon$ from [16,19,20], covering a range of temperatures from $993 - 1073\, K$. In this work, the ratio $\left(\frac{\lambda}{\tau}\right)$ is assumed to be suitably large, such that a single effective carbon diffusion field can be considered ahead of the dashed line inclined at an angle, ϕ, to the prior γ grain boundary, and is considered as a fitting parameter guided by the few observations available above.

Figure 2

For simplification of the model the following additional assumptions are made:

- α grains are assumed to nucleate instantaneously on the six corners of hexagonal γ grains at the beginning of an isothermal transformation, as shown in Figure 2. At modest undercooling and small γ grain sizes, α nucleation is dominated at γ grain corners [41].
- The interface between α and γ is assumed to consist of horizontal broad terraces and vertical risers, i.e., growth ledges (Figure 1). Solute drag and the dissipation of Gibbs energy is only considered to occur at ledge risers [42,43].

- The growth velocity normal to the effective γ/α interphase boundary is simulated using an adapted quasi-1D model developed by Chen *et al.* [44,45]. The carbon concentration and driving force for α growth is considered to be uniform about the ledge.
- The ledge is considered to nucleate in the austenite enriched in carbon immediately ahead of the interphase boundary. As the ledge nuclei is small in comparison to the size of the diffusion field of carbon the carbon concentration used to calculate the driving force for ledge nucleation is assumed to be equal to the calculated interfacial carbon concentration on the γ side of the boundary $X_C^{\gamma\alpha}$. There is no -special consideration for the influence of diffusion fields overlapping ahead of neighboring α grains.
- Any ϵ precipitation on a ledge tread does not pin the lateral movement of the ledge riser or subsequent ledge risers.

The model derived in this work takes the same basis as our previous paper [32], utilizing the recently proposed Gibbs Energy Balance (GEB) approach [44,45]. In this approach, a balance is found between the local driving force at the interfacial region [46] $\Delta G_m^{\gamma\to\alpha}$, and the dissipation of Gibbs free energy within the interphase boundary. The dissipation term ΔG_m^{disip} in this work is considered equal to the combination of the dissipation associated with solute drag ΔG_m^{SD} and a friction term ΔG_m^{frict} related to the intrinsic interphase boundary mobility, (Eqn. 2). Okamoto and Agren [40] included an additional term ΔG_m^{surf} related to the surface free energy of the ferrite grain, in this work the assumption is made that each of the γ/α interphase boundaries, although ledged are essentially flat and ΔG_m^{surf} can be neglected. As the carbon enrichment and driving force is assumed to be equal in all locations around the ledge and the dissipation of Gibbs

energy is only considered to occur at the mobile ledge risers, the Gibbs energy balance is performed in terms of a 1D interphase boundary in the direction of travel of the ledge riser. This allows for the required chemical driving force throughout the γ to α transformation, $\Delta G_m^{\gamma\to\alpha}$ to be computed.

$$\Delta G_m^{\gamma\to\alpha} = \Delta G_m^{disip}\,, \qquad \Delta G_m^{disip} = \Delta G_m^{SD} + \Delta G_m^{frict} \tag{2}$$

The GEB approach predicts the transition between transformation modes conventionally thought quite distinct. At a relatively high interfacial velocity there is little interfacial segregation, consistent with a transformation under pareqilibrium (quasi-PE) like conditions, and as the interphase boundary slows segregation of solutes becomes significant, consistent with a transformation under negligible partitioning local equilibrium like, (quasi-N-PLE) conditions.

1.2. Chemical Driving Force for Interphase Boundary Motion $\Delta G_m^{\gamma\to\alpha}$

The chemical driving force for the $\gamma \to \alpha$ transformation, $\Delta G_m^{\gamma\to\alpha}$, can be predicted as proposed by Chen *et al.* [44,45], as per the following:

$$\Delta G_m^{\gamma\to\alpha} = \sum_{i=0}^{n} X_i^0 \left(u_i^{\gamma\alpha}\left(X_i^{\gamma\alpha}\right) - u_i^{\alpha\gamma}\left(X_i^{\alpha\gamma}\right)\right) \tag{3}$$

where $u_i^{\gamma\alpha}$ and $u_i^{\alpha\gamma}$ are chemical potentials of element i at γ and α sides of the interface. It is assumed throughout this work that the molar volumes of both γ and α phases are sufficiently close, and as such, we can consider the concentrations by mole fractions. In a similar manner

to that of Chen [44,45], $X_i^{\alpha\gamma}$ and $X_i^{\gamma\alpha}$ for substitutional alloying elements are set to the be equal to the nominal concentration X_i^0, consistent with negligible partitioning of substitutional solute elements between the two matrix phases.

Considering the carbon in the remaining γ to be homogeneously distributed at any stage of the transformation, the equivalent mole fraction of carbon in the remaining γ, $\overline{X_C^\gamma}$, can be calculated by the following equation, where X_C^0 is the bulk alloying content, $f^{\alpha+\varepsilon}$, is the phase fraction of $\alpha+\epsilon$, and $X_C^{\alpha+\epsilon}$ is the carbon mole fraction in the combined pseudo phase. The consideration of $\alpha+\epsilon$ as a combined pseudo phase is not strictly true as the amount of carbon consumed by the ϵ will be variable depending upon the size, number density and the inter-sheet spacing. All of which would be expected to change dramatically throughout the course of the transformation however, it is considered that this will yield a reasonable approximation.

$$X_C^m \approx \overline{X_C^\gamma} = \frac{X_C^0 - f^{\alpha+\varepsilon} X_C^{\alpha+\epsilon}}{1 - f^{\alpha+\varepsilon}} \tag{4}$$

Assuming $\overline{X_C^\gamma}$ is a good first order approximation of X_C^m, the following set of equations can be derived. The interphase velocity of the $\gamma \rightarrow \alpha$ phase transformation can be calculated according to Zener's linearized carbon concentration gradient [47]. In this work the carbon gradient is modelled according to a quadratic function which offers a more realistic simplification of the diffusion field in the γ ahead of the interphase boundary and an improved predication of the onset of soft-impingement [48]. The interface velocity therefore can be calculated by the following equation where,

$$v = \frac{2\overline{D_C^{\gamma}}\left(X_C^{\gamma\alpha} - X_C^{m}\right)}{L\left(X_C^{\gamma\alpha} - X_C^{\alpha+\epsilon}\right)} \quad (5)$$

$X_C^{\gamma\alpha}$ is the carbon mole fraction on the γ side of the interphase boundary, $\overline{D_C^{\gamma}}$ is the diffusivity of carbon in γ. L is the diffusion length, which can be calculated in turn by Equation 6.

$$L = \frac{3\Omega(X_C^{0} - X_C^{\alpha+\epsilon})}{\left(X_C^{\gamma\alpha} - X_C^{m}\right)} \quad (6)$$

The term, $\Omega = \frac{V^{\alpha+\epsilon}}{A^{\alpha+\epsilon}}$ is the ratio of the volume of the $\alpha + \varepsilon$ pseudo-phase to its surface area. In the 2D hexagonal γ grain considered in this work this is the ratio of the area and perimeter of pseudo-phase computed using the equations A8 and A11 in the Annex.

Substituting Equation 6 into 5 and rearranging yields,

$$X_C^{\gamma\alpha} = \frac{\sqrt{3}(-\Omega v X_C^{0} - X_C^{\alpha+\epsilon})\sqrt{8\overline{D_C^{\gamma}}X_C^{\alpha+\epsilon} - 8\overline{D_C^{\gamma}}vX_C^{m} - 3\Omega v X_C^{0} + 3\Omega v X_C^{\alpha+\epsilon}} + 4\overline{D_C^{\gamma}}X_C^{m} + 3\Omega v X_C^{0} - 3\Omega v X_C^{\alpha+\epsilon}}{4\overline{D_C^{\gamma}}} \quad (7)$$

which, expresses the interfacial carbon content as a function of interphase boundary velocity. Previous solute drag models of the $\gamma \rightarrow \alpha$ transformation have been criticized as the models in question have not accounted for influence of substitutional solute elements upon the diffusivity of carbon in γ [49]. In this work the carbon diffusivity is calculated based on the full composition of the alloy, using the quasichemical thermodynamic model outlined by Bhadeshia *et al.* [50,51]. In addition, the diffusion of carbon in γ is strongly influenced by the carbon concentration in

the γ phase. In order to take account of the varying diffusion coefficient within the carbon concentration gradient ahead of the interphase boundary a weighted effective diffusion coefficient according to Trivedi and Pound [52] is considered:

$$\overline{D_C^{\gamma}} = \int_{X_C^{\gamma}=X_C^m}^{X_C^{\gamma}=X_C^{\gamma\alpha}} \frac{D_C^{\gamma}\left(X_C^{\gamma},T\right)}{X_C^{\gamma\alpha}-X_C^m} dX_C^{\gamma} \quad (8)$$

Equations 7 and 8 are solved iteratively, commencing with $\overline{D_C^{\gamma}} = D_C^{\gamma}\left(X_C^{\gamma\alpha} = X_C^m\right)$. It is found that the iterations converge after less than 10 iterations.

1.3. Dissipation of Gibbs Free Energy within the Interphase Boundary ΔG_m^{disip}

Figure 3

It has been proposed that the segregation in an interphase boundary can be described by a modified version of the triangular potential well proposed by Purdy and Bréchet [53], as shown in Figure 3, where δ is half the interphase boundary thickness and taken in this study to be equal to $0.25\,nm$, X is the solute concentration, x is the distance from the center of the interphase boundary, E_i^0 is the binding energy of the solute element. The magnitude of $\Delta E_i^{X_C^{\gamma\alpha}} = \frac{u_i^{\gamma 0} - u_i^{\alpha 0}}{2}$, where $u_i^{\gamma 0}$ and $u_i^{\alpha 0}$ are the chemical potentials of a component i in γ and α respectively, and can be calculated for each respective component as a function of the interfacial carbon content $X_C^{\gamma\alpha}$ using thermodynamic software, in this case Matcalc [31,54]. The dissipation of Gibbs free energy due to the diffusion of alloying elements inside the interphase

boundary can be determined using Cahn's equation, (Equation 9) [54] (and reviewed by Hillert in [55]) where, P is the solute drag force.

$$\Delta G_m^{SD} = PV_m = -\int_{-\delta}^{\delta} (X_i - X_i^0)\left(\frac{dE_i}{dx}\right) dx \qquad (9)$$

The concentration profile, X_i, of segregating elements within a moving interphase boundary can be described by the governing equation, Equation 10. The dissipation of Gibbs free energy is assumed to occur entirely at the mobile ledge risers. The velocity of the ledge risers is related to the velocity of the overall interphase boundary through $v_L = v\csc(\phi)$. $\overline{D_i^{\alpha\gamma}}$ is the effective i trans-interfacial diffusivity of the solute element i:

$$\frac{\partial}{\partial x}\left[\overline{D_i^{\alpha\gamma}}\frac{\partial X_i}{\partial x} + \frac{.\overline{D_i^{\alpha\gamma}}X_i}{RT}\frac{\partial E_i}{\partial x} + v_L X_i\right] = 0 \qquad (10)$$

Equation 10 is evaluated in the interphase boundary region 2δ using Equations 11 and 12 due to Purdy and Bréchet [53], which yield a substitutional element concentration profile as a function of position inside the interphase x.

$$\frac{X_i}{X_i^0} = \frac{1 + a\,exp\left(-c(1+A)\left(\frac{x}{\delta}+1\right)\right)}{1+a}, \qquad \left[-1 < \frac{x}{\delta} < 0\right] \qquad (11)$$

$$\frac{X_i}{X_i^0} = \frac{1 + \left(\frac{a(1+b)exp\left(-c(1+a)\right)}{1+a} + \frac{b-a}{1+a}\right) exp\left(-c(1+b)\frac{x}{\delta}\right)}{1+b},$$

$$\left[-1 < \frac{x}{\delta} < 0\right] \qquad (12)$$

Equations 11 and 12 are evaluated using the following three dimensionless parameters a, b and c.

$$a = \frac{\overline{D_i^{\alpha\gamma}}\left(\Delta E_i^{X_C^{\gamma\alpha}} - E_i^0\right)}{RTv_L\delta}, \qquad b = \frac{\overline{D_i^{\alpha\gamma}}\left(\Delta E_i^{X_C^{\gamma\alpha}} + E_i^0\right)}{RTv_L\delta}, \qquad c = \frac{v_L\delta}{\overline{D_i^{\alpha\gamma}}} \qquad (13A-C)$$

The trans-interfacial diffusivity remains a source of significant uncertainty. For this analysis we shall adopt a similar geometric mean methodology as Chen *et al.* [44,45]:

$$\overline{D_i^{\alpha\gamma}} = \sqrt[3]{D_i^{\alpha} D_i^{\alpha\gamma} D_i^{y}} \qquad (14)$$

where, D_i^{α} , $D_i^{\alpha\gamma}$, D_i^{y} are the diffusion coefficients of each component i in a α matrix at the interphase boundary, and within an γ matrix respectively. Matrix diffusion coefficients are readily accessible within the computational package Matcalc [31], using an appropriate mobility database. The interphase boundary diffusion coefficient is unknown, but is assumed to be very similar for all substitutional alloying elements, and close to the value for α grain boundaries derived by Fridberg *et al.* [56]. Fridberg found that the boundary diffusion coefficient of Iron is almost independent of matrix lattice structure. Moreover, Fridberg also found the diffusion coefficients of Cr, Mn, Ni and Mo are remarkably similar to the self-diffusion of iron. In this

work, Fridberg's experimentally delivered relationship (Equation 15) for the self-diffusion of iron in a boundary is used ~~the following expression is used~~ to describe the boundary diffusion of all substitutional alloying elements $D_i^{\alpha\gamma}$ ~~, generally~~. Where, δ is the half interphase boundary thickness, $D_0^{\alpha\gamma}$ is a pre-exponential term equal to $5.4 \times 10^{-14}\ m^3 s^{-1}$ and $Q_D^{\alpha\gamma}$ is the activation energy for diffusion in the interphase boundary equal to $155\ kJ\ mol^{-1}$ [56]. ~~:~~

$$2\delta D_i^{\alpha\gamma} \approx$$

$$= D_0^{\alpha\gamma} 5.4 \times 10^{-14} exp\left(\frac{-Q_D^{\alpha\gamma} 155 \times 10^3}{RT}\right) \quad m^3 s^{-1} \qquad (15)$$

The binding energy E_i^0 has been calculated using first principles Density Functional Theory (DFT) for a α $\Sigma 5$ tilt grain boundaries [57]. It will be assumed that similar values hold true for the segregation energy in the interphase boundary and regardless of interphase boundary coherency. This would appear to be reasonable given the close correspondence of the values fitted in the work of Chen *et al.* [44,45]. The average binding energy listed in (Fig. 3) the *ab-initio* study of Jin *et al.* [57] are adopted in this work, and are shown in Table 1.

Table 1

As of yet there is no fundamental evaluation of the intrinsic mobility of the γ/α interphase boundary, $M_m^{\gamma\alpha^*}$, in iron. ~~,~~ However, ~~although~~ Hillert and Höglund [58] have reviewed the experimentally fitted proposals, concluding that the equation proposed by Krielaart *et al.* [59] was the most appropriate (Equation 16). Where, $M_0^{\gamma\alpha^*}$ is a pre-exponential term equal to

$0.058\ mmol.J^{-1}\ s^{-1}$ and $Q_M^{\alpha\gamma}$ is the activation energy, which is equal to $140\ kJ\ mol^{-1}$ [60]. However, in every case reviewed the movement of the γ/α interphase boundary was assumed to be that of a smooth, planar disordered boundary, and therefore the possibility of the presence of ledges was neglected. If ledges were present the mobile risers must have an~~, which would have had risers with~~ appreciably higher mobility than Krielaart *et al.* [59] assessment. In the case of measured transformations occurring by a ledged terrace the mobility of the ledge risers $M_m^{\gamma\alpha R}$ would ~~be~~ increase the value $M_m^{\gamma\alpha^*}$ given by Equation 16~~d~~ ~~–~~by a multiplication factor of ~~by~~ $\csc(\phi)$.

$$M_m^{\gamma\alpha^*} = M_0^{\gamma\alpha^*}\ 0.058 exp\left(\frac{-Q_M^{\alpha\gamma}\ 140\times10^3}{RT}\right)\ mmol.J^{-1}\ s^{-1} \quad (16)$$

The dissipation of Gibbs free energy at the interphase boundary due to intrinsic friction, ΔG_m^{frict}, can be determined by the following equation:

$$\Delta G_m^{frict} = \frac{v_L}{M_m^{\gamma\alpha R}} \approx \frac{v}{M_m^{\gamma\alpha^*}} = \frac{v_L}{M_m^{\gamma\alpha R}} = \frac{v}{M_m^{\gamma\alpha^*}\csc(\phi)} \quad (17)$$

Combining Equations 2, 9 and 17, and assuming that the total dissipation of n substitutional alloying component can be predicted by linear summation of the individual contributions.

$$\Delta G_m^{disip} = \Delta G_m^{SD} + \Delta G_m^{frict}$$

$$= \frac{v_L}{M_m^{\gamma\alpha R} \cancel{M_m^{int}}} - \sum_{i=0}^{n} \int_{-\delta}^{\delta} (X_i - X_i^0) \left(\frac{dE_i}{dx}\right) dx \qquad (18)$$

1.4. Solving $\Delta G_m^{\gamma\to\alpha} = \Delta G_m^{disip}$

Figure 4

Figure 4 shows the adapted GEB model accounting for the variation of the interfacial carbon concentration upon the dissipation of Gibbs energy. The dissipation surface ΔG_m^{disip} is computed using the procedure as outlined in the previous section. As opposed to our previous model [32] the chemical potential of substitutional alloying elements $u_i^{\gamma 0}$ immediately ahead of the interphase boundary are evaluated as a function of the interfacial carbon content on the γ side of the interphase boundary $X_C^{\gamma\alpha}$. As shown, this has a significant effect upon the predicted dissipation of Gibbs energy especially at low interphase boundary velocities. In contrast, there is little difference in the dissipation of Gibbs energy at high velocities where solute drag is limited, with varying $X_C^{\gamma\alpha}$, this is due there being no relations known that suggest the intrinsic mobility of the interphase boundary to be a function of interfacial carbon concentration.

The solution at each distance step $\Delta G_m^{\gamma\to\alpha} = \Delta G_m^{disip}$ can be found by computing a ray for $\Delta G_m^{\gamma\to\alpha}$ for a given transformed fraction through combining Eqns. 6 – 8 and finding the intersects between this curve and the ΔG_m^{disip} surface. In some circumstances, when the transformation mode transfers from quasi-PE to quasi-NPLE, there may be several possible

intersects between the ray and the surface, in this case the model evaluates the intersect at the highest interphase boundary velocity. The highest velocity intersect is chosen as α considered to grow in the immediate vicinity of its nucleation point with a transformation under quasi-PE conditions without a solute spike in the immediate vicinity of the nucleation point.

2. Case Study – Interphase Precipitation in a V-Alloyed HSLA Steel

The development of new hot-rolled high-strength, whilst formable steels, offer the potential for novel lightweight automotive chassis components. This allows an improvement of fuel economy while, maintaining high level of passenger safety and manufacturability [60]. Hot-rolled HSLA with high strength and excellent stretch-flange formability are particularly desirable [61]. This combination of properties presents a significant challenge, requiring the optimisation of precipitation in hot-rolled HSLA. The steel industry has responded by developing single-phase ferritic steels strengthened by interphase precipitation [17,62–64]. The periodicity of these carbide precipitate rows and spacing of precipitates on each respective row strongly influences the mechanical properties through the Ashby-Orowan mechanism [62].

As with the previous paper [32], the experimental materials were provided by Tata Steel in the form of forged blocks with the composition according to Table ~~Table~~. The V-HSLA is used to study the $\gamma \rightarrow \alpha + \epsilon$ whereas, the Ref-HSLA where no strong carbide forming element is present is used as a comparison considering just the $\gamma \rightarrow \alpha$ transformation. Samples were machined into rods of $4\ mm$ diameter, $10\ mm$ length for dilatometry. Bähr-Thermoanalyse DIL 805A/D/T quenching dilatometer was used to perform all dilatometry experiments operated in vacuum and utilizing a He assisted quench. An initial heat treatment was followed for all samples consisting of heating to $1423\ K$ at $5\ Ks^{-1}$ and isothermal holding for $120\ s$ to

dissolve all pre-existing precipitates. The samples were then cooled at a rate in excess of $100\ Ks^{-1}$ to room temperature.

Table 2

The results have been supplemented with recent *a posteriori* small angle neutron scattering study upon the V-HSLA alloy in question aged varying times from 3min to 50 hours at 973 K. Taking the results extracted at the shortest aging time to be indicative of the nature of the interphase precipitates formed during the interphase precipitation mechanism (little time for further growth once within the ferritic matrix phase) suggested that the volume fraction of precipitates was in the order of 9×10^{-4} [65]. Utilizing the room temperature molar volumes for a stoichiometric VC phase and α respectively from [62] an approximation of the mole fraction of carbon within the interphase precipitates can be approximated using Eqn. 19.

$$X_C^{\epsilon} \approx f_p \frac{V_m^{\alpha}}{V_m^{\epsilon}} = 9 \times 10^{-4} \frac{7.11 \times 10^{-6}}{1.08 \times 10^{-5}} = 5.93 \times 10^{-4} \quad (19)$$

Equation 19 suggests that contrary to our assumption in our previous work [32] the consumption of carbon at the interphase is notably limited.

As the experimental alloys in this work are of low carbon content it is expected that the majority of the transformation is completed under quasi-PE conditions. Furthermore, as the measured dilatometric analysis suggests that the fraction of α measured after $5\ min$ is well below that of what would be expected from equilibrium calculations it is thought that this discrepancy in α fraction is principally due to the transition to comparatively slow quasi-NPLE transformation

kinetics. The model has therefore been systematically fit to the measured dilatometric curves by considering ϕ as a sole fitting parameter.

3. Results and Discussion

3.1. The influence of ϕ Upon the Prediction of Transformation Kinetics

Figure 5

Figure 5 shows the Influence of ϕ upon the modelled transformation kinetics for the Ref-HSLA, where the intrinsic mobility is calculated from substituting Equations 16 into 17. Increasing the value of ϕ i.e. reducing the value of $\left(\frac{\lambda}{\tau}\right)$ has the effect of shortening the period of which the transformation progresses under a quasi-PE transformation mode. This is expected as the velocity of the mobile ledge risers is related to the velocity of the overall effective interphase interface through $v_L = v\csc(\phi)$, and hence the greater the value of ϕ the slower the velocity of the ledge risers must be travelling for the overall interphase boundary to be travelling at v. The solute drag effect of substitutional alloying elements upon α growth, therefore, starts to operate at earlier transformation times. It is found in the Ref-HSLA when the incline angle $\phi \approx 0.1\ rad.\left(\frac{\lambda}{\tau} \approx \frac{1}{10}\right)$, the calculated and the measured α fractions up to 0.6 are in good agreement for transformation within 10 seconds. Accordingly, this value of ϕ is used to simulate the transformation kinetics in the V-HSLA at $973\ K$. There may be several reasons for the larger discrepancy between the calculation and the measurement for transformation times of greater than $10\ s$. The most probably is inaccuracy in the calculation of the thermodynamic driving force associated with the thermodynamic database. The

calculated final α fraction (≈ 0.85) is consistently 0.07 higher than the measured value (0.78) when the transformation time is longer than $100\,s$ the transformation approaches soft impingement. Soft impingement is realized when the carbon enriched into the remaining γ, calculated using Equation 4 (this work considers a hexagonal prior γ grain with an α grain from each corner into the center of the hexagonal prior γ grain) reaches a level such that the driving force is insufficient to intersect with the dissipation surface, even at a low interphase boundary velocity of $0.001\ nm\ s^{-1}$.

It is worth noting that in Figure 5 the transition from quasi-PE transformation mode to quasi-NPLE transformation mode is abrupt in the calculated curves using $\phi \approx 0.05\,rad.$ and $0.13\,rad.$, but it is much more continuous in the measured curve. This is because all the calculations in this workpaper are carried out using a single γ grain to save computational cost, which is important to ensure this model to be suitable for implementing in industrial environment. An weighted summation average of ferrite fraction curves calculated from running the model sequentially for using a many austenite grain size s with a size distribution will lead to themake the overall transformation curve to mode evolve more continuously. This is due to the fact that smaller austenite grains will become soft impinged earlier times and larger austenite grains as later times, respectively..

Figure 6

The transformation kinetics of the V HSLA isothermally transformed at 973 K is shown in Figure 6, where the results of the Ref HSLA also are presented for comparison. Figure 6 shows that a good correlation between the modelled volume fraction of α and dilatometric analysis of the experimental alloys during isothermal transformation at 973 K was achieved. The γ grain

diameters used for the Ref-HSLA and V-HSLA steels are the central estimates: $15.2 \pm 9.6\ \mu m$ and $12.4 \pm 6.5\ \mu m$ respectively, as reported in the previous paper [32], in both cases $\phi = \tan^{-1}\left(\frac{1}{10}\right)\ rad.$. In Figure 6, the calculated and measured α fractions up to 0.8 are in good agreement for transformation time within 20 seconds. Once again, the transformation mode changes from quasi-PE (relatively fast velocity within $10 - 20\ s$) to quasi-NPLE (relatively slow growth speed from $20\ s$ to $300\ s$). For the α formed during $100\ s$ to $300\ s$ holding time, the calculated ferrite fraction is about 8% higher than the measured value. The reason for this larger discrepancy is same as discussed before.

As shown in Figure 6, the calculated and the measured α volume fractions for both the V HSLA and the Ref HSLA agree well when isothermal holding time is shorter than 20 seconds. One can use the present model to extract the intrinsic interphase mobility by using the widely accepted value of $140{,}000\ kJmol^{-1}$ in literature as the activation energy of interphase movement. It is found that the intrinsic interphase mobility can be evaluated using Eqn. 20 this suggests that the intrinsic mobility of growth ledge risers is approximately 10 times greater than the intrinsic mobility of γ/α interphase boundaries proposed by Krielaart *et al.* [59].

$$M_m^{\gamma\alpha R} = 0.58\csc(\phi)\, exp\left(\frac{-140 \times 10^3}{RT}\right)\quad mmol.J^{-1}\,s^{-1} \qquad (20)$$

Figure 7

Figure 7 shows, the GEB Modelled progression of the dissipation of Gibbs energy for the Ref-HSLA. It is shown that when the velocity of ledge riser v_L is higher than $10^{-6}\ ms^{-1}$, the Gibbs

energy is mainly dissipated by the friction of austenite-ferrite interface and the solute drag force is negligible. However, when the ledge velocity is about $5^{-6}\ ms^{-1}$, the solute drag force reaches its maximum and plays an important role. After this the solute drag force decreases with decreasing riser velocity. As could be observed in Figure 6 there is an abrupt discontinuity in the rate of transformation in the modelled results towards the end of the transformations in each case. The reason for this discontinuity is principally the transition between quasi-PE and quasi-NPLE transformation conditions. As the model proposed in this work selects the intersect between the ΔG_m^{disip} and the $\Delta G_m^{\gamma\rightarrow\alpha}$ ray with the highest velocity in the case where several intersects are identified the discontinuity occurs at point which the modelled transformation transfers from retuning several possible intersects to a single intersect. It is thought that this could be avoided if the topology of the ΔG_m^{disip} was altered. Any one or a combination of the following parameters becoming a function of the interfacial carbon content $X_C^{\gamma\alpha}$ could achieve this: the trans interphase boundary diffusivity for substitutional solute elements $\overline{D_\iota^{\alpha\gamma}}$, the intrinsic mobility of the interphase boundary ledge risers $M_m^{\gamma\alpha R}$ or the binding energy of solute elements to the interphase boundary E_i^0.

Enomoto *et al* [66] and more recently Qiu *et al.* [67] have suggested that the binding energy of solute elements E_i^0 may be strongly influenced by the co-segregation of other solute elements through a coupled solute drag effect. Recent, atom probe tomography studies have suggested that there is significant coupled solute drag effect between carbon and manganese [68]. However, as of yet there are no published evaluations of the interaction parameters for $E_i^0\left(X_C^{\gamma\alpha}\right)$. It is noted that when such evaluations become available this could easily be integrated with the model proposed in this work.

Figure 8

Figure 8 shows the modelled evolution of the inter-sheet spacing of interphase precipitates in the V-HSLA as a function of the perpendicular distance from the prior γ grain boundary h. Taking the interfacial energy of the γ/α interphase boundary to be $\sigma = 0.55\,Jm^{-2}$ the inter-sheet spacing is calculated through Eqn. 1 and is found to correlate well with the measured inter-sheet spacing previously reported of $19 \pm 2\,nm$ [32]. The first inflection in the modelled inter-sheet spacing $@h \approx 0.75\,\mu m$ attributable to the change of the geometry of the growing α grains, from a mode of 6 growing triangles located at the prior γ boundary corners to a mode where these triangles have coalesced and the remaining γ is a shrinking hexagon. The second inflection at $@h \approx 3.00\,\mu m$ is due to the change in transformation mode at the ledge risers from quasi-PE to quasi-NPLE. The continual increase in inter-sheet spacing after $h \approx 3.00\,\mu m$ is caused by the rapid onset of soft impingement. If the γ grain size were to be significantly larger than that of the cases studies considered in this work the onset of soft impingement would be delayed and an extended period of relatively stable inter-sheet spacing would be observed, similar to what is often observed experimentally where grain sizes of typically $r_0 = 200\,\mu m$ [69]. In this case, the model geometry outlined in Fig. 2 could be adapted to consider the effect of many α grains growing from γ boundary faces by approximating the net effective mobile γ/α interphase interface is parallel to the prior γ grain boundary.

4. Summary

A model is presented using an adapted version of the solute drag model of Purdy and Bréchet, an evolved version based upon the GEB concept, and the theory of the diffusional formation

of super-ledges by Bhadeshia. The original GEB model proposed by Chen and Van der Zwaag [45] has been adapted to introduce the effect of a ledged interphase boundary. Furthermore, the model has been extended to incorporate the effect of the variable $X_C^{\gamma\alpha}$ upon the chemical potential of substitutional alloying elements $u_i^{\gamma 0}$in the γ immediately ahead of the interphase boundary. The dissipation of Gibbs energy at the interphase boundary ΔG_m^{disip} are evaluated as a function of the interfacial carbon content on the γ side of the interphase boundary $X_C^{\gamma\alpha}$ and the velocity of the interphase boundary ledge risers v_L producing a 3D dissipation surface rather than the 2D curve in the original GEB model. It has been possible to draw the following conclusions:

1) The α fraction transformed at $973\ K$ in both the Ref and V-HSLA steels is simulated to be in excellent agreement with the measured dilatometry. Although, the modelled final α fraction ≈ 0.88 remains slightly higher than the measured ≈ 0.8. This is thought to be probably due to uncertainty in several key parameters such as the binding energy of solute elements to the interphase boundary.
2) The isothermal ferrite transformation kinetics in both the V HSLA and Ref HSLA steels exhibits two stages: fast growth (ferrite volume fraction from 0 to about 0.7) under quasi-PE and slow growth (α fraction from 0.7 to 0.8) under quasi-NPLE. The calculations showed that the solute drag force due to the segregation of substitutional solute elements on the austenite-ferrite interphase is the primary reason for the latter growth mode.
3) Through the systematic fitting of ϕ it is suggested that the intrinsic mobility of growth ledge risers is 10 times greater than the previously experimentally derived assessment

of the intrinsic mobility for disordered γ/α interphase boundaries proposed by Krielaart *et al.* [59].

4) The sheet spacing of interphase precipitation in the vanadium micro-alloyed low carbon steel isothermally transformed at $973\ K$ and is simulated to vary between $14\ [nm]$ and $24\ [nm]$ considering a fitted realistic γ/α interfacial energy of $\sigma = 0.55\ [Jm^{-2}]$ this is in good agreement with the $(19 \pm 2\ nm)$ measured using TEM.

Acknowledgements

Authors are thankful to Dr Arjan Rijkenberg from Tata Steel for providing the experimental material. Financial support from the EPSRC grant EP/L018632/1 "Micro-structuring micro-alloyed steels via non-metallic precipitate formation" and financial assistance from the WMG Centre High Value Manufacturing Catapult are gratefully acknowledged.

References

1) H. I. Aaronson: in *Decompos. Austenite by Diffus. Process. Proc. a Symp. Held Philadelphia, Pennsylvania, Oct. 19, 1960 under Spons. Ferr. Metall. Comm. Inst. Met. Div. Metall. Soc.*, V. F. Zackay and H. I. Aaronson, eds., Interscience Publishers, New York, (~~(~~1962)~~)~~.

2) J. R. Bradley, J. M. Rigsbee, and H. I. Aaronson: *Metall. Trans. A*, **8**~~,~~ (1977), 323~~–~~~~33~~.

3) D V Edmonds and R W K Honeycombe: *Met. Sci.*, **12**~~,~~ (1978), 399~~–~~~~405~~.

4) G. R. Purdy: *Acta Metall.*, **26**~~,~~ (1978), 477~~–~~~~86~~.

5) M. Onink, F. D. Tichelaar, C. M. Brakman, E. J. Mittemeijer, and S. van der Zwaag: *J. Mater. Sci.*, **30**~~,~~ (1995), 6223~~–~~~~34~~.

6) H. I. Aaronson: *J. Microsc.*, **102**, (1974), 275–300.

7) Hubert Aaronson: *Metall. Mater. Trans. A*, **24**, (1993), 241–76.

8) G J Shiflet, M a Mangan, and W G Meng: *Interface Sci.*, **6**, (1998), 133–54.

9) H. I. Aaronson, W. T. Reynolds, and G. R. Purdy: *Metall. Mater. Trans. A*, **35**, (2004), 1187–1210.

10) H. I. Aaronson, T. Furuhara, M. G. Hall, J. P. Hirth, J. F. Nie, G. R. Purdy, and W. T. Reynolds: *Acta Mater.*, **54**, (2006),, 1227–32.

11) Cyril S Smith: *Trans. Am. Soc. Met.*, **45**, (1953), 533–75.

12) G Kurdjumov and G Sachs: *Z. Phys*, **64** ,(1930), 325–43.

13) Z. Nishiyama: *Sci. Reports Res. Institutes, Tohoku Univ.*, **23**, (1934), 637–64.

14) G Wasserman: *Eisenhuettenwes*, **16**, (1933), 647.

15) R. W. K. Honeycombe: *Metall. Trans. A*, **7**, (1976), 915–36.

16) A T Davenport and R W K Honeycombe: *Proc. R. Soc. London Ser. a-Mathematical Phys. Sci.*, **322**, (1971), 191–205.

17) T. N. Baker: *Mater. Sci. Technol.*, **25**, (2009), 1083–1107.

18) H. I. Aaronson, M. R. Plichta, G. W. Franti, and K. C. Russell: *Metall. Trans. A*, **9**, (1978), 363–71.

19) K. Campbell and R. W. K. Honeycombe: *Met. Sci.*, **8**, (1974), 197–203.

20) R.A. Ricks and P.R. Howell: *Acta Metall.*, **31**, (1983), 853–61.

21) H-W. Yen, P-Y. Chen, C-Y. Huang, and J-R. Yang: *Acta Mater.*, **59**, (2011), 6264–74.

22) T. Furuhara and H. I. Aaronson: *Scr. Metall.*, **22**, (1988), 1635–37.

23) T. Furuhara, A. M. Dalley, and H. I. Aaronson: *Scr. Metall.*, **22**, (1988), 1509–14.

24) T. Furuhara and H. I. Aaronson: *Acta Metall. Mater.*, **39**, (1991), 2887–99.

25) Tadashi Furuhara and Tadashi Maki: *Mater. Trans. JIM*, **33**, (1992), 734–39.

26) John W Cahn: *Acta Metall.*, **8**, (1960), 554–62.

27) T. B. Massalski, D. E. Laughlin, and W. A. Soffa: *Metall. Mater. Trans. A*, **37**, (2006), 825–31.

28) K. R. Kinsman, E. Eichen, and H. I. Aaronson: *Metall. Trans. A*, **6**, (1975), 303–17.

29) H.I. Aaronson, M. Enomoto, and J. K. Lee: *Mechanisms of Diffusional Phase Transformations in Metals and Alloys*, (2010).

30) H. K. D. H. Bhadeshia: *Phys. Status Solidi a-Applied Res.*, **69**, (1982), 745–50.

31) Ernst Kozeschnik and Bruno Buchmayr: in *Math. Model. Weld Phenom. 5*, H-H. Cerjak and H.K.D.H. Bhadeshia, eds., London Institute of Materials, (2001), 349–61.

32) Samuel Clark, Vit Janik, Yongjun Lan, and Seetharaman Sridhar: *ISIJ Int.*, **57**, (2017), 524–532.

33) M-Y. Chen, M. Gouné, M. Militzer, Y. Bréchet, and J-R. Yang: *Metall. Mater. Trans. A*, **45**, (2014), 5351–61.

34) C. Atkinson: *Proc. R. Soc. London A*, **378**, (1981), 351–68.

35) C. Atkinson: *Proc. R. Soc. London A*, **384**, (1982), 107–33.

36) M. Enomoto: *Acta Metall.*, **35**, (1987), 935–45.

37) M. Enomoto: *Acta Metall.*, **35**, (1987), 947–56.

38) M Enomoto and H I Aaronson: *Scr. Metall.*, **23**, (1989), 1983–88.

39) M. Enomoto and J. P. Hirth: *Metall. Mater. Trans. A*, **27A**, (1996), 1491–1500.

40) R. Okamoto and J. Ågren: *Acta Mater.*, **58**, (2010), 4791–4803.

41) M Militzer, R Pandi, and EB Hawbolt: *Metall. Mater. Trans. A*, **27**, (1996), 1547–56.

42) H. I. Aaronson, S. K. Liu, W. T. Reynolds Jr, and G. J. Shiflet: *J. Mater. Sci.*, **20**, (1985), 4232–38.

43) Yves Bréchet and Gary Purdy: *Scr. Mater.*, **52**, (2005), 7–10.

44) H. Chen, K. Zhu, L. Zhao, and S. van der Zwaag: *Acta Mater.*, **61**, (2013), 5458–68.

45) H. Chen and S. van der Zwaag: *Acta Mater.*, **72**, (2014), 1–12.

46) J. Odqvist, B. Sundman, and J. Ågren: *Acta Mater.*, **51**, (2003), 1035–43.

47) Clarence Zener: *J. Appl. Phys.*, **20**, (1949), 950–53.

48) H. Chen and S. Van Der Zwaag: *J. Mater. Sci.*, **46**, (2011), 1328–36.

49) H K D H Bhadeshia: *J. Mater. Sci.*, **18**, (1983), 1473–81.

50) H K D H Bhadeshia: *Met. Sci.*, **15**, (1981), 477–80.

51) S S Babu and H K D H Bhadeshia: *J. Mater. Sci. Lett.*, **14**, (1995), 314–16.

52) R. Trivedi and G. M. Pound: *J. Appl. Phys.*, **38**, (1967), 3569–76.

53) G. R. Purdy and Y. J. M. Bréchet: *Acta Metall. Mater.*, **43**, (1995), 3763–74.

54) J. W. Cahn: *Acta Metall.*, **10**, (1962), 789–98.

55) M. Hillert: *Acta Mater.*, **47**, (1999), 4481–4505.

56) J. Fridberg, L.E. Torndahl, and M. Hillert: *Jernkontorets Ann*, **153**, (1969), 263–76.

57) H. Jin, I. Elfimov, and M. Militzer: *J. Appl. Phys.*, **115**, (2014), 93506
.

58) M. Hillert and L. Höglund: *Scr. Mater.*, **54**, (2006), 1259–63.

59) GP Krielaart, J Sietsma, and S van der Zwaag: *Mater. Sci. Eng. A*, **237**, (1997), 216–23.

60) C. M. Sonsino: *Materwiss. Werksttech.*, **38**, (2007), 9–22.

61) R. A. Rijkenberg, A. Blowey, P. Bellina, and C. Wooffindin: *4th Int. Conf. Steels Cars Truck. June 15-19, Braunschweig, Ger.*, (2014), 426–33.

62) T. Gladman: *The Physical Metallurgy of Microalloyed Steels*, 2nd Editio, Institute of Materials, London, (2002).

63) Y. Funakawa, T. Shiozaki, K. Tomita, T. Yamamoto, and E. Maeda: *ISIJ Int.*, **44**, (2004), 1945–51.

64) R. Lagneborg, B. Hutchinson, T. Siwecki, and S. Zajac: *The Role of Vanadium in Microalloyed Steels*, 2nd ed., Swerea KIMAB, Stockholm, (2014).

65) Y.Q. Wang, S. Clark, V. Janik, R.K. Heenan, D. Alba Venero, K. Yan, D.G. McCartney, S. Sridhar, and P. D. Lee: *Acta Mater.*, **145**, (2018), 84–96.

66) M. Enomoto, C. L. White, and H. I. Aaronson: *Metall. Trans. A*, **19**, (1988), 1807–18.

67) C. Qiu, H. S. Zurob, and C. R. Hutchinson: *Acta Mater.*, **100**, (2015), 333–43.

68) H. P. Van Landeghem, B. Langelier, D. Panahi, G. R. Purdy, C. R. Hutchinson, G. A. Botton, and H. S. Zurob: *Jom*, **68**, (2016), 1329–34.

69) T. Murakami, H. Hatano, G. Miyamoto, and T. Furuhara: *ISIJ Int.*, **52**, (2012), 616–25.

Appendix

Appendix 1 - 2D geometric description of ledged terraces within a hexagonal γ grain

Area of original γ grain:

$$A_0 = \frac{3\sqrt{3}{r_0}^2}{2} \quad (A1)$$

Perpendicular height of α growth ledge nucleation point from the prior γ grain boundary:

$$h = S\left(\cot(\phi) + \tan\left(\frac{\pi}{6} + \phi\right)\right)\sin(\phi) \quad (A2)$$

Fraction transformed:

$$f^{\alpha+\epsilon} = \frac{A^{\alpha+\varepsilon}}{A_0} \quad (A3)$$

Fraction transformed $f^{\vartriangle^*}$ at which the geometry of the growing ferritic phase changes from growing triangles to a shrinking hexagon of remaining γ:

$$f^{\vartriangle^*} = \frac{\cos(2\phi) + \sqrt{3}\sin(2\phi) - 1}{\cos(2\phi) + \sqrt{3}\sin(2\phi) + 2} \quad (A4)$$

Transformed distance$S^{\vartriangle^*}$ from ferritic phase nucleation point, S, at which the geometry of the growing ferritic phase changes from growing triangles to a shrinking hexagon of remaining γ:

$$S^{\Delta^*} = \frac{r_0}{\left(\csc(\phi) + \sec\left(\frac{\pi}{6} + \phi\right)\right)} \quad (A5)$$

Growing Triangles: $S \leq S^{\Delta^*}$, $f \leq f^{\Delta^*}$

Transformed distance from ferritic phase nucleation point, S, for a given transformed fraction:

$$S = \frac{r_0\sqrt{\frac{f\sqrt{3}}{2}}}{\sqrt{\cot(\phi) + \tan\left(\frac{\pi}{6} + \phi\right)}} \quad (A6)$$

Area of transformed prior γ grain:

$$A^{\alpha+\varepsilon} = 3S^2\left(\cot(\phi) + \tan\left(\frac{\pi}{6} + \phi\right)\right) \quad (A7)$$

Transformed volume to surface area ratio:

$$\Omega = \frac{S}{2} \quad (A8)$$

Shrinking Hexagon: $S \geq S^{\Delta^*}$, $f \geq f^{\Delta^*}$

Transformed distance from ferritic phase nucleation point, S, for a given transformed fraction:

$$S = \frac{r_0\left(2\cos\left(\phi - \frac{\pi}{6}\right) - \sqrt{3 - 3f}\right)}{2} \quad (A9)$$

Area of transformed prior γ grain:

$$A^{\alpha+\varepsilon} = A_0 - 2\sqrt{3}\left(S - r_0\cos\left(\phi - \frac{\pi}{6}\right)\right)^2 \quad (A10)$$

Transformed volume to surface area ratio:

$$\Omega = \frac{2\sqrt{3}\left(S - r_0\cos\left(\phi - \frac{\pi}{6}\right)\right)^2 - \left(\frac{3\sqrt{3}{r_0}^2}{2}\right)}{4\sqrt{3}\left(S - r_0\cos\left(\phi - \frac{\pi}{6}\right)\right)} \quad (A11)$$

Appendix 2 – Nomenclature

$\overline{D_C^{\gamma}}$	Effective diffusion coefficient of carbon in γ considering the carbon concentration gradient
$\overline{D_i^{\alpha\gamma}}$	Effective diffusion coefficient of element i in an α/γ interphase boundary (geometric mean)
$\overline{X_C^{\gamma}}$	Effective homogeneous carbon mole fraction in the remaining untransformed γ
ΔE_i	Half chemical potential difference of element i over the γ/α interphase boundary
D_C^{γ}	Diffusion coefficient of carbon in γ
D_i^{α}	Diffusion coefficient of element i in α
$D_i^{\alpha\gamma}$	Diffusion coefficient of element i in an α/γ interphase boundary
D_i^{γ}	Diffusion coefficient of element i in γ
D_i	Effective γ/α interphase boundary diffusion coefficient for element i
E_i^0	Binding energy of the solute element i to the γ/α interphase boundary
$M_m^{\gamma\alpha^*}$	Intrinsic γ/α interphase boundary mobility
r_0	γ grain radius
$u_i^{\alpha 0}$	Chemical potential of element i with a mole fraction of X_i^{α} in α
$u_i^{\alpha\gamma}$	Chemical potential of element i on the α side of the γ/α interphase boundary
$u_i^{\gamma 0}$	Chemical potential of element i with a mole fraction of X_i^{γ} in γ

$u_i^{\gamma\alpha}$	Chemical potential of element i on the γ side of the γ/α interphase boundary
v_L	Ledge riser velocity
V_m	Molar volume of iron
v_T	Ledge tread velocity
X_C^0	Bulk carbon mole fraction
X_C^m	Mole fraction of carbon in the center of the γ grain
$X_C^{\alpha\gamma}$	Mole fraction of carbon on the α side of the γ/α interphase boundary
$X_C^{\gamma\alpha}$	Mole fraction of carbon on the γ side of the γ/α interphase boundary
X_i^0	Bulk mole fraction of alloying element i
X_i^α	Mole fraction of element i in forming α
$X_i^{\alpha\gamma}$	Mole fraction of element i on the α side of the γ/α interphase boundary
X_i^γ	Mole fraction of element i in forming γ
$X_i^{\gamma\alpha}$	Mole fraction of element i on the γ side of the γ/α interphase boundary
$X_i(x)$	Mole fraction of element i in the interphase with respect to distance from the center of the interphase boundary x
ΔG_m^{disip}	Total dissipation of Gibbs energy in the γ/α interphase boundary
ΔG_m^{frict}	Dissipation of Gibbs energy in the interphase due to intrinsic interphase mobility
ΔG_m^{SD}	Dissipation of Gibbs Energy due to the diffusion of substitutional alloying elements in the interphase boundary
ΔG_m^{surf}	Dissipation of Gibbs energy due to surface free energy
$\Delta G_m^{\gamma\to\alpha}$	Molar driving force for the $\gamma \to \alpha$ transformation
A	Area
f	Phase fraction

h	Perpendicular distance from the prior γ grain boundary
i	Alloying element i.e. Mn, Si, V, ect….
L	Diffusion length of carbon ahead of the γ/α interphase boundary
n	Total number of alloying elements in the alloy
P	Solute drag force
R	Universal gas constant
S	α growth distance from the nucleation point
t	Time
T	Absolute temperature
v	Overall effective Interface velocity
V_m	Molar volume
x	Distance from γ/α interphase boundary center
δ	Half interphase boundary thickness
λ	Inter-sheet spacing of interphase precipitates
σ	Interfacial energy of the γ/α interphase boundary
τ	Inter-ledge-riser spacing i.e. length of ledge tread
ϕ	Ledge terrace incline angle
Ω	Ratio of product phase volume to product phase surface area

1

2

Captions List:

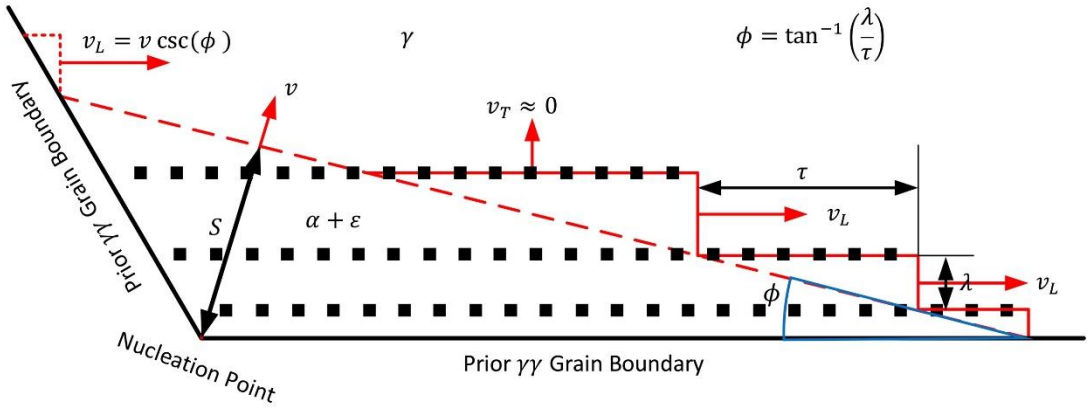

Figure 1 Schematic depiction of an α ledge terrace at an γ grain boundary corner with interphase precipitates ϵ (Online version in color.)

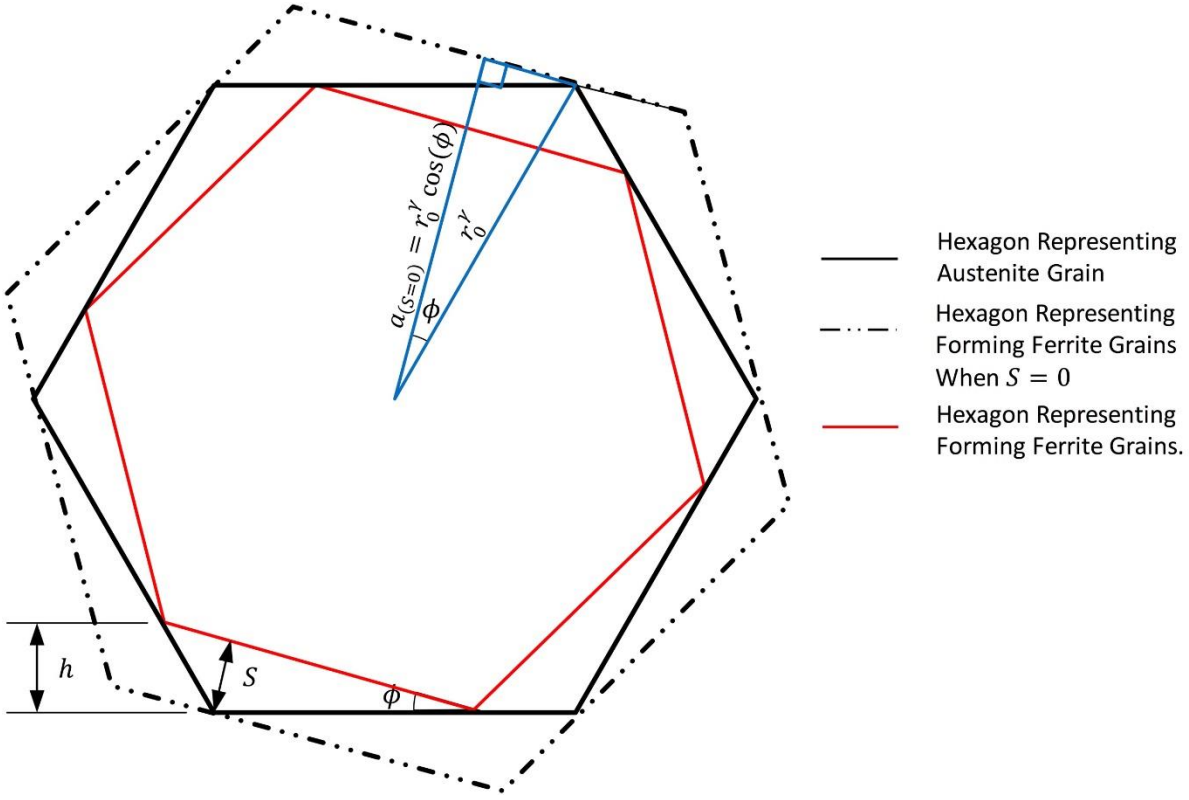

1

2 **Figure 2 2D Geometric description of the $\gamma \rightarrow \alpha$ transformation (Online version in color.)**

3

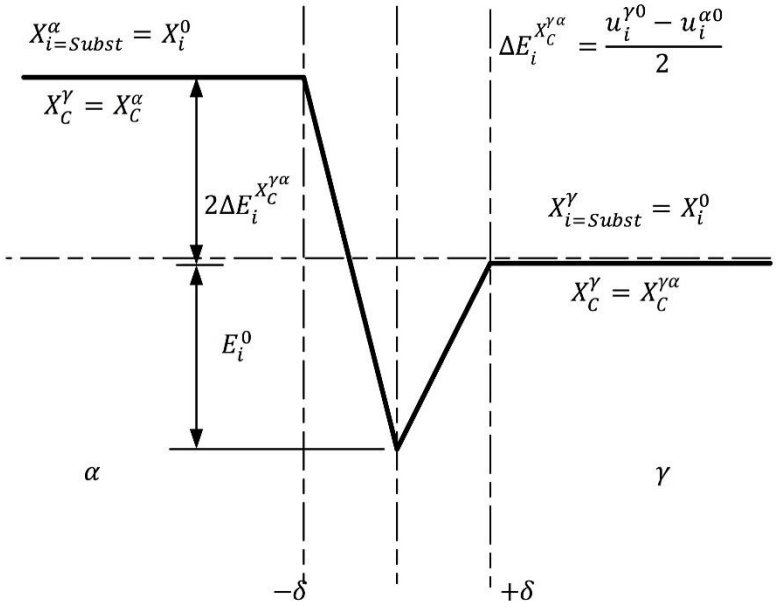

Figure 3 Schematic of a modified Purdy-Bréchet interphase boundary potential well for a general γ stabilizing component.

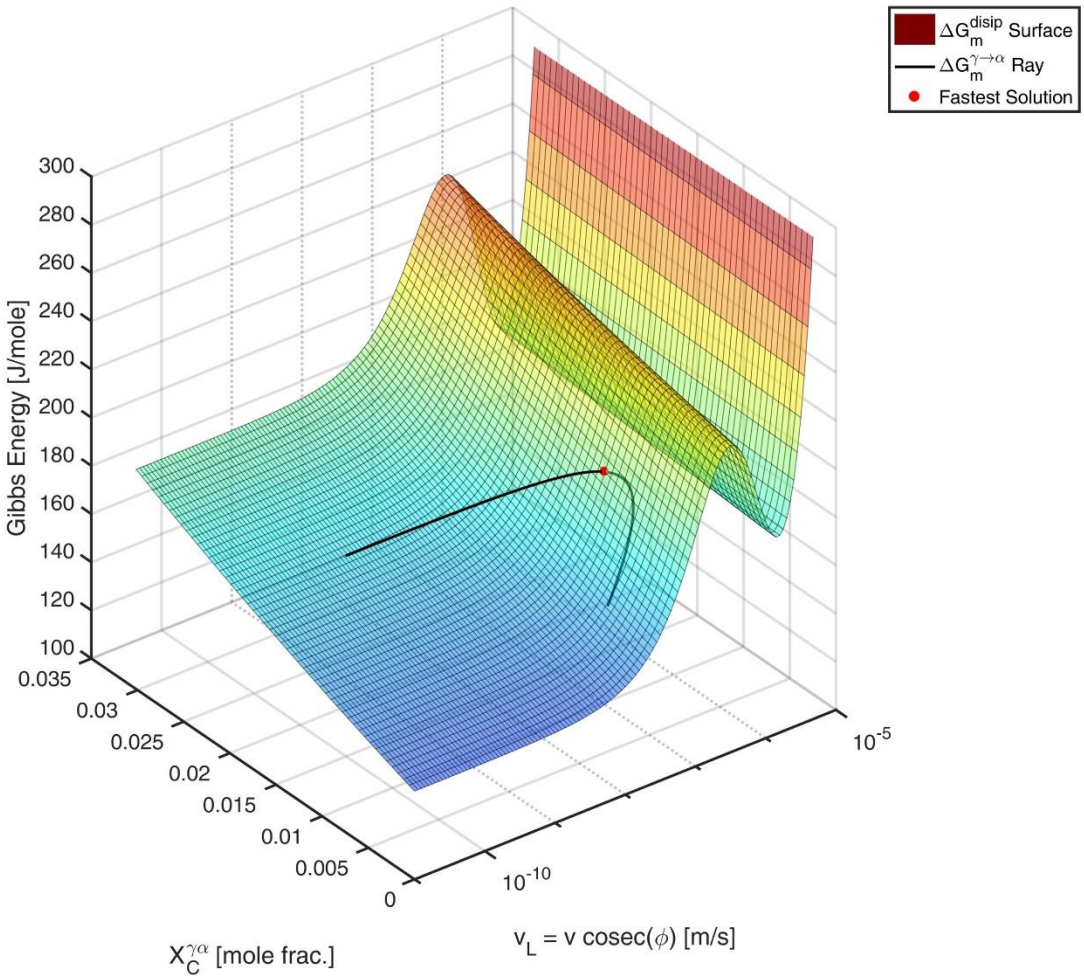

1

2 **Figure 4 Modified GEB model accounting for the variation of the interfacial carbon**

3 **concentration upon the dissipation of Gibbs Energy shown for the Ref-HSLA (Online**

4 **version in color.)**

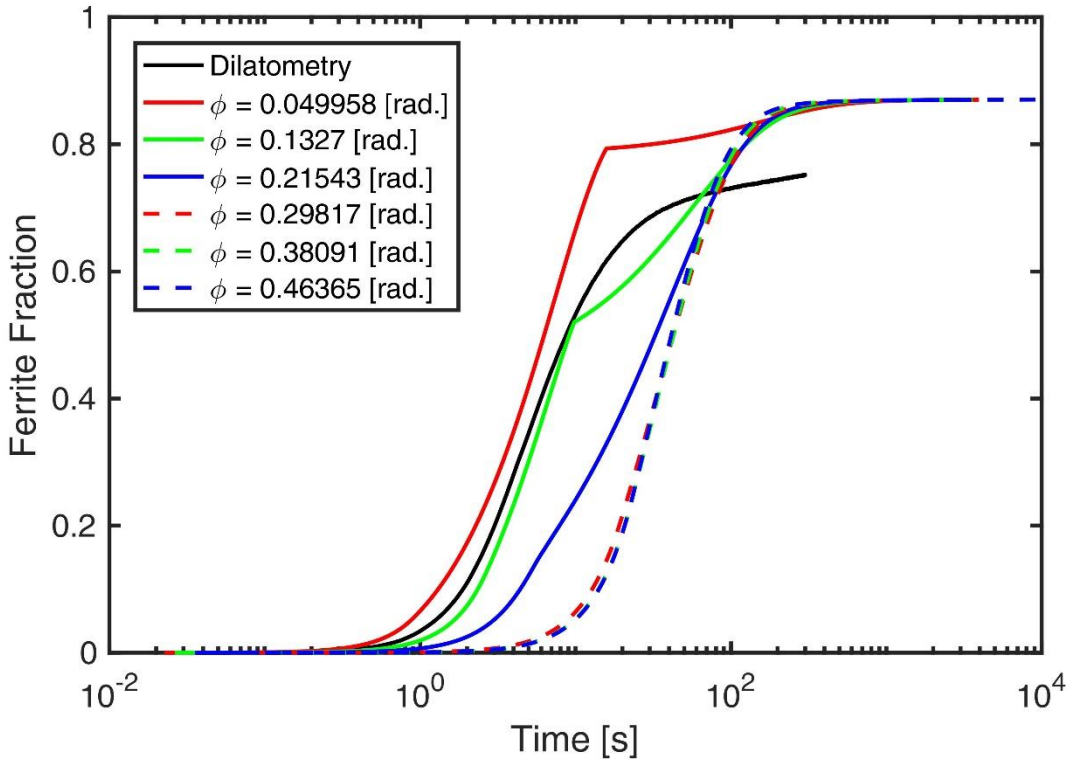

Figure 5 Influence of the Variable $\boldsymbol{\phi = \tan^{-1}\left(\frac{\lambda}{\tau}\right)}$ upon Modelled Transformation Kinetics for the Ref-HSLA (Online version in color.)

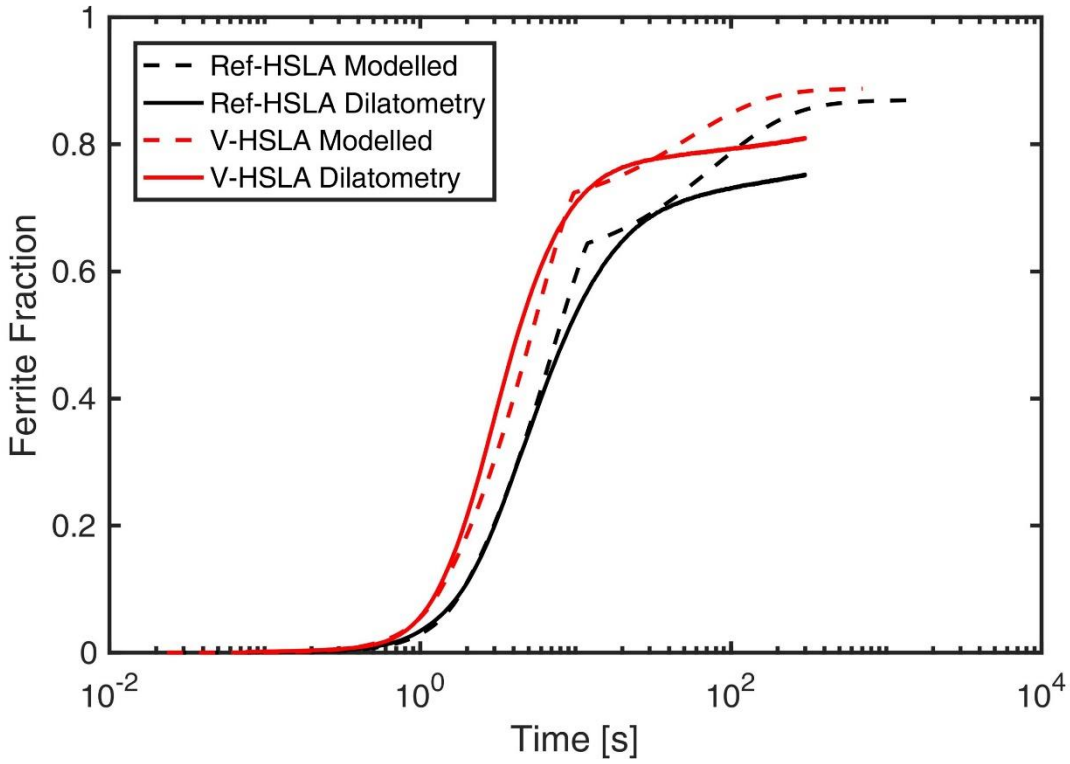

Figure 6 Correlation between the modelled volume fraction and dilatometric analysis of the experimental alloys during isothermal transformation at $973\ K$ (Online version in color.)

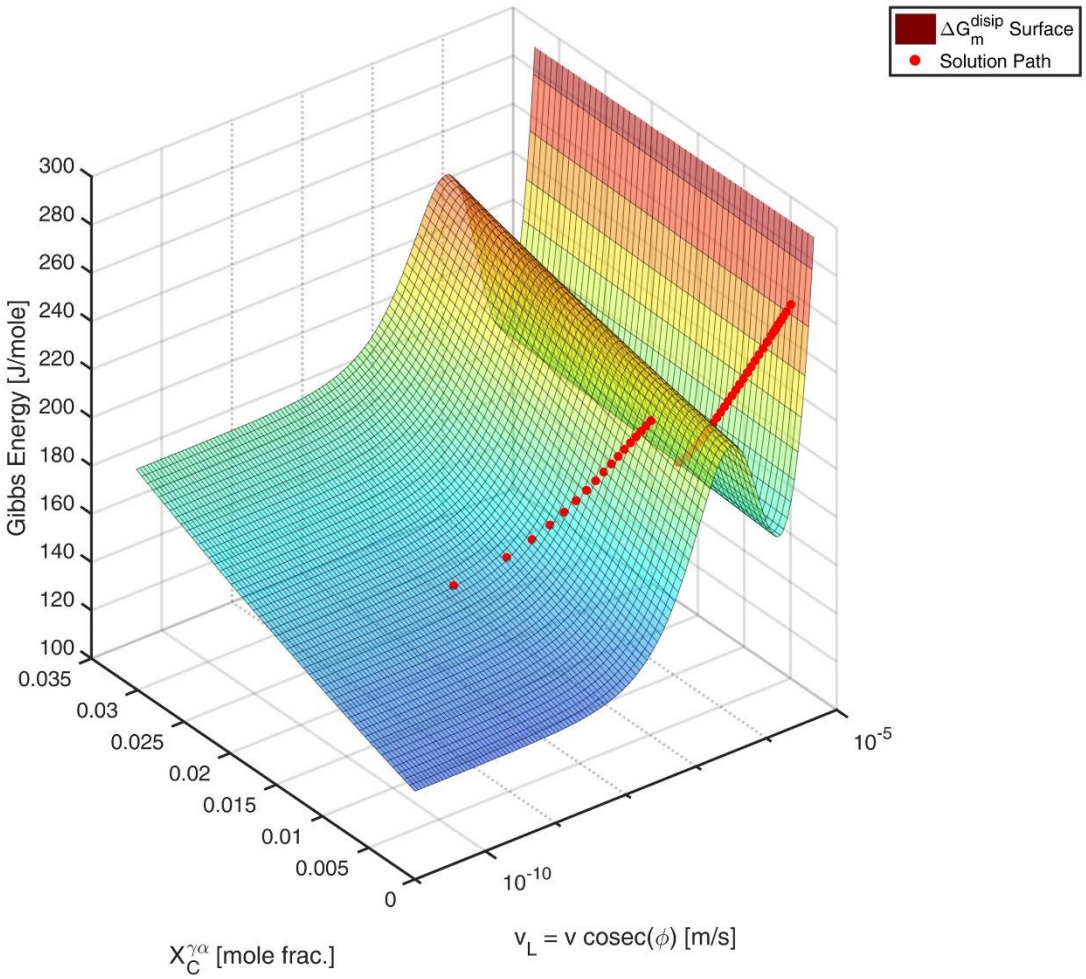

Figure 7 GEB Modelled progression of the dissipation of Gibbs energy for the Ref-HSLA isothermally transformed at $973\ K$ (every tenth solution displayed) (Online version in color.)

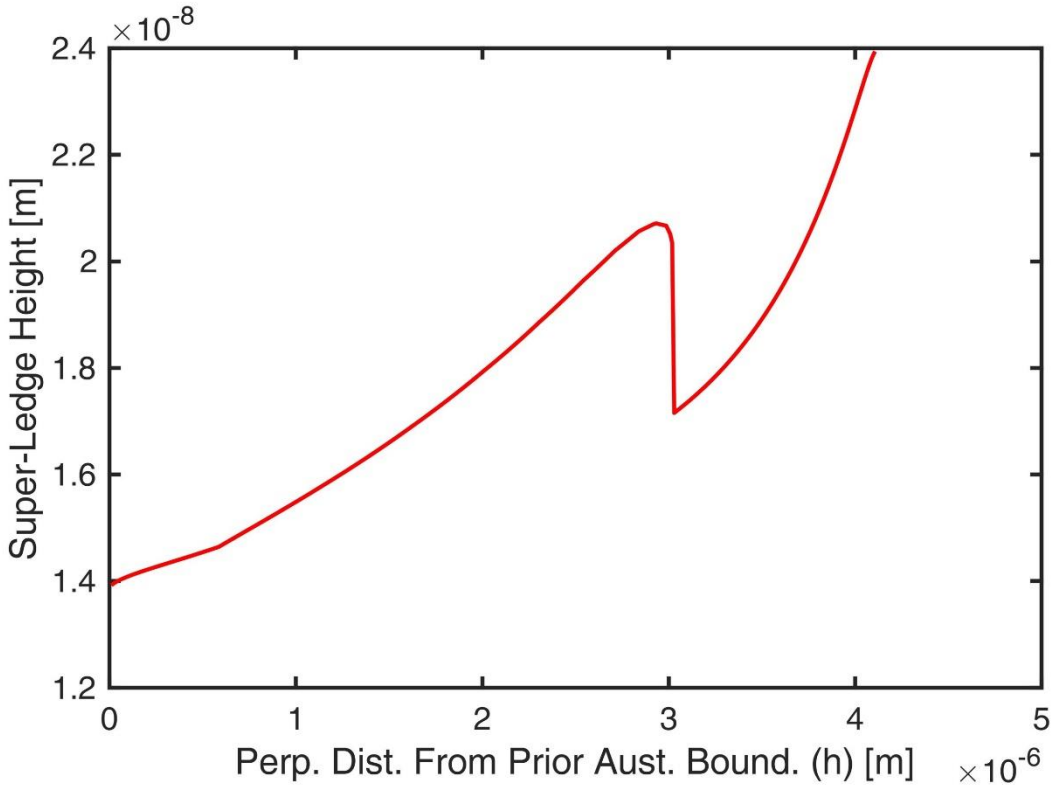

Figure 8 Modelled evolution of inter-sheet spacing/growth-ledge height for V-HSLA during isothermal transformation at $973\ K$ (Online version in color.)

Table 1 Binding energies adopted for segregation calculations for elements relevant in this study.

Element i	$E_i^0\ kJ\ mol^{-1}$
Mn	10.6
V	7.7
Si	6.8

Table 2 Experimental Alloy Compositions

Element	Ref. HSLA*wt*%	V HSLA *wt*%
Mn	1.60	1.60
Si	0.20	0.18
V	~	0.20
C	0.038	0.047